Available online at www.eccomasproceedia.org
Eccomas Proceedia COMPDYN (2023) 4265-4285

ECCOMAS
Proceedia

COMPDYN 2023
9th ECCOMAS Thematic Conference on
Computational Methods in Structural Dynamics and Earthquake Engineering
M. Papadrakakis, M. Fragiadakis (eds.)
Athens, Greece, 12-14 June 2023

SENSITIVITY TO DAMPING IN NONLINEAR DYNAMIC ANALYSIS

Terje Haukaas[1]

[1] Professor, Dept. of Civil Engineering, The University of British Columbia, Vancouver
6250 Applied Science Lane, Vancouver, BC, V6T 1Z4, Canada
e-mail: terje@civil.ubc.ca

Abstract

Exact response sensitivities are derived and calculated for nonlinear dynamic analysis with Rayleigh damping formulated in terms of the current tangent stiffness matrix. The derivations show that the third-order tensor formed by the derivative of the tangent stiffness matrix with respect to the displacement vector is required. That quantity is non-zero only for material models that feature nonlinearity in at least a portion of their stress-strain curve. Bilinear models do not have that characteristic. The Bouc-Wen material model is selected in this paper to verify the implementations. That model exhibits a smooth transition between the elastic and the yield state. In order to obtain correct response sensitivities, it is necessary to let the third-order tensor amend the coefficient matrix of the system of equations that produce the sensitivity results. This paper also presents exact response sensitivities for modal damping and Rayleigh damping with coefficients implicitly specified as a target damping at two natural frequencies. Eigenvalue derivatives are implemented in order to calculate results for those cases. The amendment of the coefficient matrix is then asymmetric. Examples are presented to show the sensitivity of the displacement response with respect to four groups of parameters: material properties, cross-section geometry, mass, and parameters of the damping model.

Keywords: Response sensitivity analysis, Direct differentiation method, Nonlinear dynamic structural analysis, Rayleigh damping, Modal damping, Bouc-Wen material model.

ISSN:2623-3347
Peer-review under responsibility of the organizing committee of COMPDYN 2023.
doi: 10.7712/120123.10717.20068

1 INTRODUCTION

Nonlinear dynamic analyses are computationally demanding. That is one reason why it is desirable to learn as much as possible from every analysis. One instrument for adding insight beyond the response is the calculation of response sensitivities. Response sensitivities have value even when the confidence in the response is low. For example, the response derivatives may reveal that the response is highly sensitive to an input parameter that is associated with substantial uncertainty. That would prompt caution, as well as investigations related to that parameter. The fundamental objective in this paper is to derive, implement, and calculate exact response sensitivities in an efficient manner. Pioneered at the University of Iowa [1][2][3][4][5] and extended at the University of California at Berkeley[6][7][8], the direct differentiation method is adopted in this paper. It facilitates the efficient calculation of response sensitivities in parallel with the calculation of the response. The results from the direct differentiation method are exact once the derivative equations are correctly implemented on the computer.

Three specific objectives are addressed in this paper. First, exact response sensitivities are derived, implemented, and calculated for situations where the damping matrix is formulated in terms of the current tangent stiffness and, hence, the current displacement. Second, response sensitivities are obtained for situations where the user specifies the target damping on selected natural frequencies. One example is the use of Rayleigh damping with a target damping ratio specified at two natural frequencies. Another example addressed in this paper is the modal damping matrix, which entails the specification of a target damping on some or all of the natural frequencies. In both cases, it is necessary to differentiate the dynamic eigenvalue problem for the structure. The third objective is to visualize and verify the response sensitivity results, and to present applications other than gradient-based reliability and optimization analysis.

The scope of this paper includes displacement-based frame elements with fiber-discretized sections and one uniaxial material model in each fiber. Derivatives of the displacement response are calculated with respect to nodal masses, material parameters, and cross-section shape parameters. Shape sensitivities associated with nodal coordinates are not included here. The scope of the paper also includes the differentiation of the response equations for a specific Bouc-Wen material model. That model is employed because it exhibits smooth transitions from elastic to yield. That is significant because the derivations in this paper show that the derivative of the tangent stiffness of the material with respect to the strain is required in the response sensitivity calculations. Based on work by Baber and Noori [9], the author implemented a somewhat complex Bouc-Wen model featuring degradation in OpenSees [10] in the early 2000s. A more transparent model was later implemented in OpenSees by Schellenberg et al. [11] based on work by Casciati [12]. That implementation is extended in the present work. The Bouc-Wen model was originally formulated by Wen [13], who referenced a 1967 conference paper by R. Bouc. Early work on this model was also presented by Baber and Wen [14].

This paper is organized in the manner that the actual derivation & implementation work progressed. Starting with developments for the Bouc-Wen material model, followed by its use in static then dynamic analysis, this paper tours the lessons learned to establish the implementation of correct response sensitivity calculations.

2 ELEMENTS, SECTIONS, MATERIALS

A modest but transparent finite element model is employed to demonstrate the developments presented in this paper. The steel column shown in Figure 1 is utilized, discretized into five displacement-based nonlinear frame elements. Each element has five integration points, formulated as wide-flange sections, located along the element according to the Lobatto quadrature rule. As shown in Figure 1, each cross-section has two integration points in each flange, and

eight integration points in the web. The results presented in this paper are obtained with L=15m, h_w=355mm, t_w=11mm, b_f=365mm, t_f=18mm, and $M=(A\rho)L/5$=392.1kg, where A is the section area and ρ=7,850kg/m^3 is the mass density. Combined with the initial stiffness value given in the next paragraph, this gives the column a first natural period of 0.52 sec.

Each integration point in each section contains a hysteretic uniaxial material model. As mentioned earlier, the Bouc-Wen model is selected in order to highlight issues related to the direct differentiation method for Rayleigh damping with the current tangent stiffness. That material model takes six input parameters: E, f_y, α, γ, β, and η. Specifically, E is the modulus of elasticity, here set to 200GPa; f_y is the yield stress, here set to 350MPa; α is the strain hardening, here set to 2%. The two "Bouc-Wen parameters" γ and β are set equal to 0.5. The integer η governs the sharpness of the transition from elastic to yield. The value η=3 is used throughout this paper, except in the next paragraph.

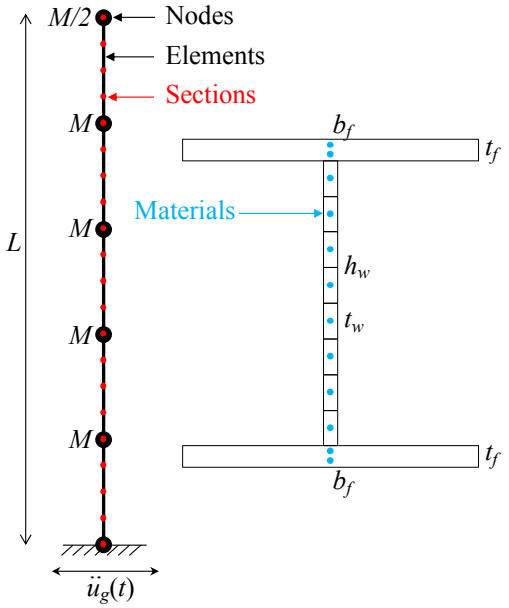

Figure 1: Structural model.

Figure 2 shows stress-strain curves for different values of η. The smooth transition from the elastic state to plastic flow is clearly visible. The higher value of η, the sharper the transition is. The stress-strain curves shown in Figure 2 are obtained by recording the stress when the strain is varied as a sine-function with 1% amplitude. For that to be achieved, only the stress response is required. That is insufficient for the calculation of response sensitivities. In fact, it is insufficient even for nonlinear static and dynamic analysis, because the algorithmically consistent tangent, i.e., the derivative of the stress with respect to the strain is missing. That issue and others are addressed in the implementations made in this work.

The two previously mentioned implementations of the Bouc-Wen model are made in the open-source framework OpenSees [10]. That object-oriented software framework created in C++ was spearheaded in the late 1990s by Dr. Fenves and his then PhD student Dr. McKenna. Around the same time, Dr. Fenves taught a course on nonlinear structural analysis, for which he developed a miniature version of OpenSees in Matlab, which labelled G2, because OpenSees was then called G3. The author of the present paper took that course and recently translated G2 into the Python programming language. It is an extended Python version of G2 that is employed

to obtain the results presented in this paper. The extended Python version of G2 is posted on the author's research website, terje.civil.ubc.ca, along with notes and examples.

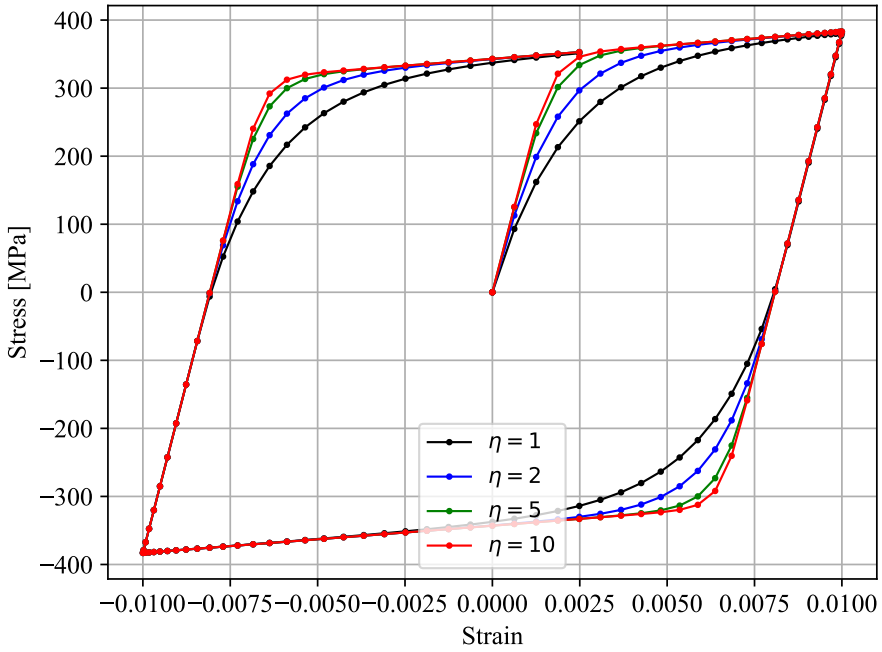

Figure 2: Material model.

3 CONSISTENT TANGENT

In nonlinear analysis, static and dynamic, an accurate tangent stiffness ensures optimal convergence towards equilibrium in the Newton-Raphson algorithm. Errors in the tangent leads to slow convergence, or no convergence at all. In this paper it is stressed that the tangent stiffness also appears in the system of equations that govern the response sensitivities. As a result, an inaccurate tangent stiffness leads to inaccurate response sensitivity results.

It is not only bugs in the implementation that can cause accuracy problems in the sensitivity results, associated with the tangent stiffness. The use of the "continuum tangent" instead of the algorithmically consistent tangent leads to slower convergence and also inaccurate response sensitivity results. An example, suppose the cantilever column in Figure 1 is subject to a uniformly distributed lateral load with intensity 10kN/m. Tracking the top tip displacement as the load increases produces a distinctly nonlinear load-displacement curve, not shown here for brevity. Significant yielding occurs after the load increases beyond 6kN/m. The derivative of that tip displacement with respect to the modulus of elasticity is shown in Figure 3. In that figure, and throughout this paper, black dots identify sensitivity results obtained by the finite difference method. That method entails the rerunning of each analysis with a perturbed parameter value in order to estimate, in an approximate manner, the derivative of the displacement with respect to the input value. The black dots in Figure 3 are obtained by rerunning the nonlinear static analysis with the value of the modulus of elasticity perturbed by 10^{-8} times its original value. The maximum difference between that approximate result and the blue line, which is obtained by the direct differentiation implementations in this work, is $2.3 \cdot 10^{-18}$ m/Pa. That is reasonable accuracy, because Figure 3 shows that the response sensitivity is in the order of $1.5 \cdot 10^{-11}$ m/Pa. Notice that the response sensitivity result obtained with the *continuum* tangent, shown as a red line in Figure 3 and derived shortly, exhibits significant error. Adding to the appeal of the algorithmically consistent tangent is that the number of iterations of the

Newton-Raphson algorithm in the ten load increments is 3, 5, 5, 6, 6, 7, 7, 7, 7, 7 with the algorithmically consistent tangent and 5, 7, 11, 14, 17, 22, 31, 32, 19 with the continuum tangent.

To understand the difference between the continuum tangent and the consistent tangent, consider the stress of the Bouc-Wen model, written

$$\sigma = \alpha \cdot E \cdot \varepsilon + (1-\alpha) \cdot f_y \cdot z \tag{1}$$

where z varies during the analysis and governs the hysteretic response. The sought tangent is

$$\frac{d\sigma}{d\varepsilon} = \alpha \cdot E + (1-\alpha) \cdot f_y \cdot \frac{dz}{d\varepsilon} \tag{2}$$

The differential equation that governs the evolution of z is

$$\dot{z} = \frac{1}{\varepsilon_y} \cdot (\dot{\varepsilon} - \gamma \cdot \dot{\varepsilon} \cdot |z|^\eta - \beta \cdot |\dot{\varepsilon}| \cdot z^\eta) \tag{3}$$

where $\varepsilon_y = f_y/E$=yield strain, and γ, β, and η are material parameters. Implemented by Schellenberg et al. [11], ε_y here serves as a scaling factor to provide a transition from elastic to yielding at appropriate strain values. When the sum of γ and β equal unity then z varies between –1 and 1. The choice $\gamma = \beta = 0.5$ is appropriate for a bilinear material with smooth transitions; examples with other values are shown in the first figure in the paper by Wen [13] and elsewhere.

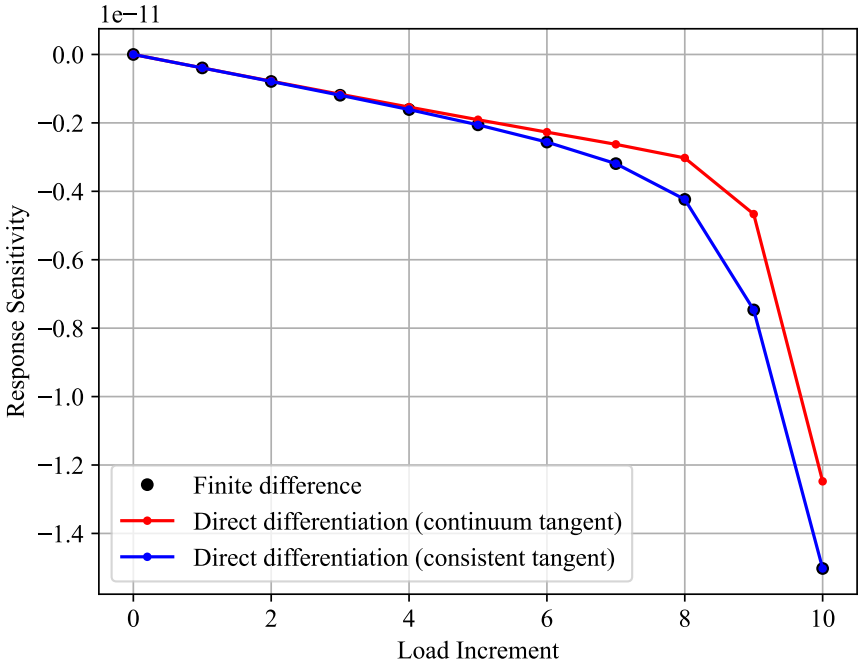

Figure 3: Derivative of tip displacement with respect to modulus of elasticity.

The Backward Euler algorithm, generically written $z_{n+1} = z_n + \Delta t\, r(z_{n+1})$, where r is the right-hand side, is utilized to solve the differential equation in Eq. (3). The relevant right-hand side, i.e., that of Eq. (3), is first reorganized by pulling the strain rate outside the parenthesis:

$$\dot{z} = \frac{1}{\varepsilon_y} \cdot \left(1 - \left(\gamma + \beta \cdot \text{sign}(\dot{\varepsilon} \cdot z)\right) \cdot |z|^\eta\right) \cdot \dot{\varepsilon} \tag{4}$$

That right-hand side is then substituted into the Backward Euler algorithm, which then reads

$$z_{n+1} = z_n + \frac{1}{\varepsilon_y} \cdot \left(1 - \left(\gamma + \beta \cdot \text{sign}(\dot{\varepsilon}_{n+1} \cdot z_n)\right) \cdot |z_{n+1}|^\eta\right) \cdot (\varepsilon_{n+1} - \varepsilon_n) \tag{5}$$

because Δt cancels. To solve Eq. (5) for z_{n+1}, which appears on both sides of the equal sign, the Newton algorithm, generically written $x_{j+1}=x_j-f(x_j)/f'(x_j)$ is employed. The function f is the right-hand side of Eq. (5), once z_{n+1} is moved to that side, and prime means derivative with respect to z_{n+1}.

Once the Newton algorithm that determines z_{n+1} converges, the tangent is sought. For reference, the continuum version of the derivative $dz/d\varepsilon$ in Eq. (2) is obtained by first using the chain rule of differentiation to state the basic fact that

$$\dot{z} = \frac{dz}{dt} = \frac{dz}{d\varepsilon}\frac{d\varepsilon}{dt} = \frac{dz}{d\varepsilon}\dot{\varepsilon} \tag{6}$$

A comparison between Eq. (4) and Eq. (6) immediately reveals the expression for $dz/d\varepsilon$, which is substituted into Eq. (2) to produce the continuum tangent. The consequence of using that tangent is inaccurate response sensitivity results, as suggested by the red line in Figure 3.

The algorithmically consistent version of $dz/d\varepsilon$ can be obtained in two ways. First, recognize that any change in z_{n+1} results from a change in the fraction f/f' that appears in the Newton algorithm. As a result, the differentiation of f/f' with respect to ε_{n+1} yields the correct derivative to be substituted into Eq. (2). Another approach is to differentiate Eq. (5) with respect to ε_{n+1} and solving for $dz_{n+1}/d\varepsilon_{n+1}$. Both approaches give the same result, but the latter approach is preferred in this paper. That is because the repeated differentiation of Eq. (5) is adopted when additional derivatives are sought later in the paper.

4 THE DIRECT DIFFERENTIATION METHOD

Let the lateral displacement at the top of the cantilevered column in Figure 1 be denoted by $u(t)$, where t is time. Furthermore, let one of the input parameters, for example M, E, f_y, α, or a cross-section dimension, be denoted by the generic symbol θ. The objective of the direct differentiation method is to calculate $du(t)/d\theta$ in an exact and efficient manner. In order to do so, consider the system of governing equilibrium equations

$$\mathbf{M}\ddot{\mathbf{u}} + \mathbf{C}\dot{\mathbf{u}} + \tilde{\mathbf{F}}(\mathbf{u}) = \mathbf{F} \tag{7}$$

where $\mathbf{M}$=mass matrix, $\mathbf{C}$=damping matrix, $\tilde{\mathbf{F}}$=internal resisting forces, $\mathbf{F}$=external loads, and $\mathbf{u}$ is the displacements vector, which contains the tracked displacement u. Each superimposed dot means one derivative with respect to time. The nonlinear dependence of $\tilde{\mathbf{F}}$ on $\mathbf{u}$ is shown; subsequent derivations address the situation where $\mathbf{C}$ is also a function of $\mathbf{u}$. Eq. (7) represents a spatial discretization of the structural boundary value problem in terms of elements connected to degrees of freedom collected in the vector $\mathbf{u}$. A temporal discretization of the initial value problem is introduced by means of the following generic time-stepping scheme:

$$\ddot{\mathbf{u}}_{n+1} = a_1\mathbf{u}_{n+1} + a_2\mathbf{u}_n + a_3\dot{\mathbf{u}}_n + a_4\ddot{\mathbf{u}}_n \tag{8}$$

$$\dot{\mathbf{u}}_{n+1} = a_5\mathbf{u}_{n+1} + a_6\mathbf{u}_n + a_7\dot{\mathbf{u}}_n + a_8\ddot{\mathbf{u}}_n \tag{9}$$

where a_i are constants. In the analyses behind this paper, the Newmark algorithm with γ=0.5 and β=0.25 is employed. Here, the symbols γ and β must not be confused with the identical symbols used in the Bouc-Wen model. The selected discretization implies that $a_1=1/(\beta\,\Delta t^2)$, $a_2=-a_1$, $a_3=-1.0/(\beta\,\Delta t)$, $a_4=1-1/(2\beta)$, $a_5=\gamma/(\beta\,\Delta t)$, $a_6=-a_5$, $a_7=1-\gamma/\beta$, and $a_8=\Delta t\,(1-\gamma/(2\beta))$. In order to obtain $du(t)/d\theta$, Eqs. (8) and (9) are substituted into Eq. (7) followed by the differentiation of the result with respect to θ. Before embarking on those steps, special attention is given to the differentiation of $\tilde{\mathbf{F}}$. The reason is that $\tilde{\mathbf{F}}$ depends on θ implicitly via $\mathbf{u}$ and also potentially explicitly via the algorithm that calculates and assembles $\tilde{\mathbf{F}}$. This is symbolically written $\tilde{\mathbf{F}}(\mathbf{u}(\theta),\theta)$ and the chain rule of differentiation yields [6]

$$\frac{\partial \tilde{\mathbf{F}}}{\partial \mathbf{u}} \cdot \frac{\partial \mathbf{u}}{\partial \theta} + \left.\frac{\partial \tilde{\mathbf{F}}}{\partial \theta}\right|_{\mathbf{u}\text{ fixed}} = \frac{\partial \mathbf{F}}{\partial \theta} \tag{10}$$

For hysteretic problems it is necessary to calculate all components of the vector $d\mathbf{u}/d\theta$ in order to calculate $du/d\theta$. The vector $d\mathbf{u}/d\theta$ appears in Eq. (10). This is kept in mind when Eqs. (8) and (9) are now substituted into Eq. (7), followed by differentiation and reorganization of the result to obtain, at time step n+1:

$$\left(a_1\mathbf{M} + a_5\mathbf{C} + \frac{\partial \tilde{\mathbf{F}}_{n+1}}{\partial \mathbf{u}_{n+1}}\right)\frac{\partial \mathbf{u}_{n+1}}{\partial \theta} =$$

$$\frac{\partial \mathbf{F}_{n+1}}{\partial \theta} - \frac{\partial \mathbf{M}}{\partial \theta}(a_1\mathbf{u}_{n+1} + a_2\mathbf{u}_n + a_3\dot{\mathbf{u}}_n + a_4\ddot{\mathbf{u}}_n) - \mathbf{M}\left(a_2\frac{\partial \mathbf{u}_n}{\partial \theta} + a_3\frac{\partial \dot{\mathbf{u}}_n}{\partial \theta} + a_4\frac{\partial \ddot{\mathbf{u}}_n}{\partial \theta}\right) -$$
$$\frac{\partial \mathbf{C}}{\partial \theta}(a_5\mathbf{u}_{n+1} + a_6\mathbf{u}_n + a_7\dot{\mathbf{u}}_n + a_8\ddot{\mathbf{u}}_n) - \mathbf{C}\left(a_6\frac{\partial \mathbf{u}_n}{\partial \theta} + a_7\frac{\partial \dot{\mathbf{u}}_n}{\partial \theta} + a_8\frac{\partial \ddot{\mathbf{u}}_n}{\partial \theta}\right) - \left.\frac{\partial \tilde{\mathbf{F}}(\mathbf{u}_{n+1})}{\partial \theta}\right|_{\mathbf{u}_{n+1}\text{ fixed}} \tag{11}$$

where ground motion loading means that the load vector derivative is

$$\frac{\partial \mathbf{F}_{n+1}}{\partial \theta} = -\frac{d\mathbf{M}}{d\theta} \cdot \boldsymbol{\Gamma} \cdot \ddot{u}_{g,n+1} \tag{12}$$

where $\ddot{u}_g$ is the ground acceleration in the horizontal direction, at time t_{n+1}, and $\boldsymbol{\Gamma}$ is the mass participation vector. After convergence of the Newton-Raphson algorithm at each time increment, the linear system of equations in Eq. (11) is solved for $d\mathbf{u}/d\theta$. The coefficient matrix in that system is $a_1\mathbf{M} + a_5\mathbf{C} + \left(\partial \tilde{\mathbf{F}}_{n+1}/\partial \mathbf{u}_{n+1}\right) \equiv a_1\mathbf{M} + a_5\mathbf{C} + \mathbf{K}_{n+1}$, which is identical to the effective tangent stiffness employed in the iterations of the Newton-Raphson algorithm. Eq. (11) is implemented in G2, leading to the results presented in this paper. What is presented thus far leads to the following summary of the direct differentiation method:

1) The method is associated with a one-time cost to implement Eq. (11) in the nonlinear finite element analysis code. The derivation and correct implementation of $\partial \tilde{\mathbf{F}}_{n+1}/\partial \theta$ for fixed current displacements can be demanding; that task is addressed in subsequent sections. The differentiation of the damping matrix, $\mathbf{C}$, may also require careful attention; that task is also addressed in subsequent sections.

2) The method gives exact and algorithmically consistent results. No approximations are involved in the derivations and implementations.

3) The method is efficient because Eq. (11) is a linear system of equations. Solvers that factorize the coefficient matrix once, followed by solutions for different right-hand sides, further reduces the computational cost. Nonetheless, it is noted that Eq. (11) must be solved for each parameter, θ, at every time increment when hysteretic material models are present.

4) The method benefits from avoiding the Modified Newton-Raphson approach, characterized by not updating the stiffness during the iterations. In the proper Newton-Raphson algorithm, the tangent stiffness is recalculated in each iteration, benefitting the direct differentiation method because it requires the current tangent stiffness after convergence, in order to solve Eq. (11). Developments presented in this paper produce amendments to that coefficient matrix before Eq. (11) is solved.

5) The method requires two calls to each hysteretic material instance, at every time step, beyond the ordinary state determination of the Newton-Raphson algorithm. As stressed by Zhang & Der Kiureghian [6], the calculation of $\partial\tilde{\mathbf{F}}_{n+1}/\partial\theta$ for fixed current displacements, stemming from Eq. (10), prompts two "phases" of the sensitivity calculations. In Phase 1 the elements, sections, and materials are called to produce contributions to $\partial\tilde{\mathbf{F}}_{n+1}/\partial\theta\big|_{\mathbf{u}_{n+1}\text{ fixed}}$ in order to form the right-hand side of Eq. (11). Because the calculations are for fixed displacements at increment n+1 but *not* at increment n and earlier, it is necessary to store the unconditional derivative of the history variables of the materials *without* the assumption of fixed displacements. That is referred to as Phase 2, conducted after Eq. (11) is solved for $d\mathbf{u}_{n+1}/d\theta$. The storage of unconditional derivatives of history variables must accommodate one entry for every θ.

The method requires care when calculating $\partial\tilde{\mathbf{F}}_{n+1}/\partial\theta\big|_{\mathbf{u}_{n+1}\text{ fixed}}$, for at least two reasons. First, the algorithm for the material state determination may be intricate, with bug-prone sensitivity implementations as a result. Second, the requirement for the conditional derivative is that $\mathbf{u}_{n+1}$ is fixed, not that ε_{n+1} is fixed. This is emphasized because when θ represents a cross-section dimension, which is relevant in this paper, then the strain changes with θ even when $\mathbf{u}_{n+1}$ is fixed. This point is elaborated upon in subsequent sections.

6) The method requires the following amendment to the Newton-Raphson algorithm of nonlinear analysis:

Upon convergence, at each time increment, n+1, before committing the state:

- Ensure that the algorithmically consistent tangent stiffness is up-to-date
- Loop over the θ-variables for which response sensitivities are sought
  - Phase 1: Assemble the right-hand side of Eq. (11) for the relevant θ by calculating the conditional derivative of the stress and other internal forces for fixed displacement $\mathbf{u}_{n+1}$ but *not* fixed $\mathbf{u}_n$ and not necessarily fixed ε_{n+1}
  - Solve Eq. (11) for $\partial\mathbf{u}_{n+1}/\partial\theta$
  - Phase 2: Send $\partial\mathbf{u}_{n+1}/\partial\theta$ to elements, sections, and materials in order to calculate the unconditional derivative of all hysteretic history variables for the relevant θ
- Commit the converged state, i.e., store history variables, as well as their unconditional derivatives calculated in Phase 2

5 BOUC-WEN DERIVATIVES, PART I

At this stage, before damping is addressed, it is clear that each material instance must at least be able to produce the conditional derivative $d\sigma/d\theta|_{\varepsilon_{n+1}\text{ fixed}}$ and store the unconditional derivative of the history variables, once $\partial\varepsilon_{n+1}/\partial\theta$ is available. For the Bouc-Wen model, this is accomplished by differentiating Eqs. (1) and (5). The first reads

$$\left.\frac{d\sigma_{n+1}}{d\theta}\right|_{\varepsilon_{n+1}\text{ fixed}} = \frac{d\alpha}{d\theta}\cdot E\cdot\varepsilon_{n+1} + \alpha\cdot\frac{dE}{d\theta}\cdot\varepsilon_{n+1}$$
$$-\frac{d\alpha}{d\theta}\cdot f_y\cdot z_{n+1} + (1-\alpha)\cdot\frac{df_y}{d\theta}\cdot z_{n+1} + (1-\alpha)\cdot f_y\cdot\left.\frac{dz_{n+1}}{d\theta}\right|_{\varepsilon_{n+1}\text{ fixed}} \quad (13)$$

Differentiation of Eq. (5) with respect to θ yields a somewhat lengthy expression with $dz_{n+1}/d\theta$ on both sides of the equal sign. As an example of the derivatives that appear is $d|z_{n+1}|^{\eta}/d\theta$, which evaluates to $\eta\,|z_{n+1}|^{\eta-1}\cdot\text{sign}(z_{n+1})\cdot dz_{n+1}/d\theta$. In the end, solving for $dz_{n+1}/d\theta$ yields the result required in Eq. (13). That result is implemented in G2 and its correctness is verified in Figure 3. Its correctness is also verified in subsequent plots because it serves as a foundation for the developments presented later.

6 SECTION DERIVATIVES, PART I

The result presented for $du/d\theta$ in Figure 3, for $\theta=E$, carries the simplicity that E is a parameter of the material model. An additional point is now made for situations where θ is one of the cross-section parameters, i.e., h_w, b_f, t_f, or t_w. To that end, consider the section integration

$$\widetilde{\boldsymbol{F}}_s = \sum_{j=1}^{N_{\text{fib}}}(\mathbf{T}_{ms}\cdot A\cdot\sigma) \tag{14}$$

where the section force vector, $\widetilde{\boldsymbol{F}}_s=[M,\ N]^{\text{T}}$, contains the bending moment, M, and the axial force, N, N_{fib} is the number of fibers in the cross-section, and $\mathbf{T}_{ms}=[-y,\ 1]^{\text{T}}$ is the kinematic transformation between the material level and the section level, entering the relationship $\varepsilon=\mathbf{T}_{ms}\mathbf{u}_s$. The symbol y denotes the location of the fiber relative to the centroid. The cross-section parameters h_w and t_f affect y. In that case, the complete derivative of the section forces, sought in Eq. (11), reads

$$\left.\frac{\partial\widetilde{\boldsymbol{F}}_s(\mathbf{u}_{s,n+1})}{\partial\theta}\right|_{\mathbf{u}_{s,n+1}\text{ fixed}} = \sum_{j=1}^{N_{\text{fib}}}\left(\frac{\partial\mathbf{T}_{ms}}{\partial\theta}\cdot A\cdot\sigma_{n+1}+\mathbf{T}_{ms}\cdot\frac{\partial A}{\partial\theta}\cdot\sigma_{n+1}+\mathbf{T}_{ms}\cdot A\cdot\left(\frac{\partial\sigma_{n+1}}{\partial\varepsilon_{n+1}}\cdot\frac{\partial\varepsilon_{n+1}}{\partial\theta}+\left.\frac{\partial\sigma_{n+1}}{\partial\theta}\right|_{\varepsilon_{n+1}\text{ fixed}}\right)\right) \tag{15}$$

where $d\sigma_{n+1}/d\varepsilon_{n+1}$ is the stiffness of the material. The derivative $d\varepsilon_{n+1}/d\theta$ is carefully observed to be $(d\mathbf{T}_{ms}/d\theta)\mathbf{u}_s$, which involves the derivative of y with respect to the cross-section parameter. For that reason, the implicit dependence of the stress via the strain in the last parenthesis in Eq. (15) is important for the accuracy of response derivatives calculated with respect to h_w and t_f. Figure 4 included to emphasize that point; it shows the derivative of the tip displacement with respect to h_w. When $d\varepsilon_{n+1}/d\theta=d\mathbf{T}_{ms}/d\theta\,\mathbf{u}_s$ is included in Eq. (15), leading to the result shown as a blue line in Figure 4, then the result matches the finite difference results shown by black dots. In contrast, omitting $d\varepsilon_{n+1}/d\theta$ leads to the inaccurate result shows as a red line in Figure 4.

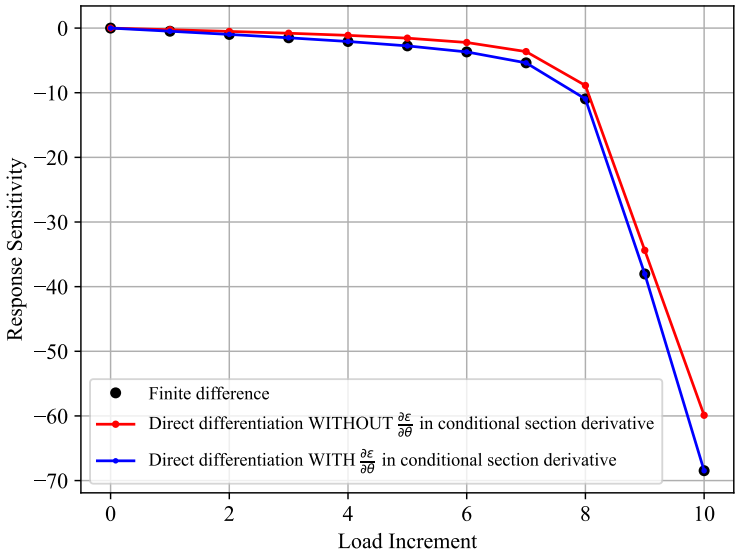

Figure 4: Inaccuracy in response sensitivity result when missing the chain rule of differentiation in Eq. (15).

The derivations presented thus far facilitate the plot of response sensitivities shown in Figure 5, obtained from the same nonlinear static analysis that produced Figure 3. Figure 5 shows the derivative of the tip displacement for three material parameters and four cross-section parameters. As before, black dots are finite difference results, provided to check the accuracy of the direct differentiation implementation, which product the colored lines. A scaling is conducted to facilitate the plotting of all results in one figure. Specifically, each variable is assigned at 10% coefficient of variation, which means that its standard deviation is 10% of the values provided earlier. Figure 5 shows the derivatives $du/d\theta$ multiplied by its respective standard deviation. The choice of a uniform coefficient of variation equal to 10% is made in order to provide transparent results. If the reader wishes to apply a smaller coefficient of variation to the geometry parameters, for instance, then that is achieved by scaling the relevant lines in Figure 5. With the uniform coefficient of variation, the web height is the most important parameter, followed by the flange width. The yield stress also ranks high. Note also that all parameters featured in Figure 5 are "resistance parameters," in the sense that increasing their value decreases the displacement response. The remainder of the paper deals with dynamic analysis.

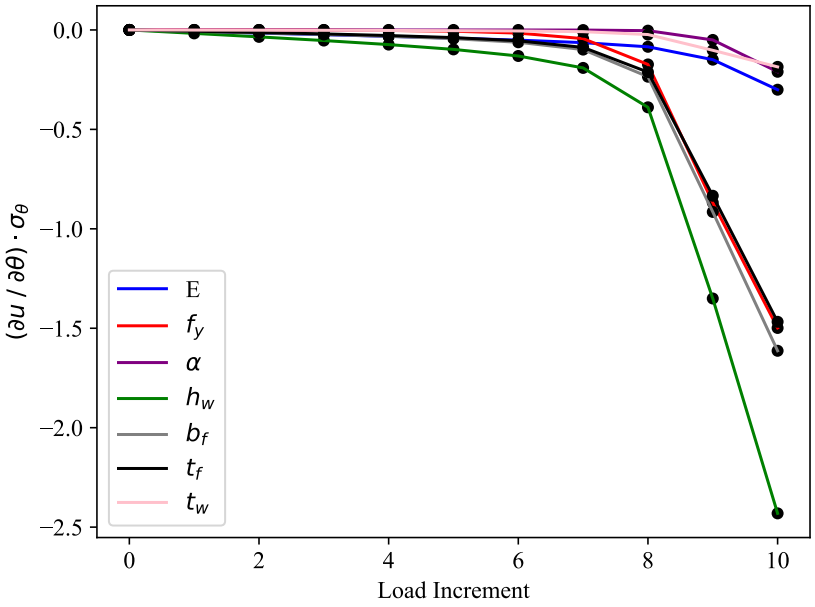

Figure 5: Derivatives $du/d\theta$ multiplied by the respective standard deviation of θ.

To demonstrate the items presented already, in the context of dynamics, the cantilevered column in Figure 1 is subjected to an artificial impulse-type ground motion. It consists of a single sine-wave lasting from t=0 to t=0.5sec. with maximum amplitude 7g at t=0.25sec. The ground acceleration is zero after t=0.5sec. That ground motion is intended to cause significant yielding, thereby testing the derivations and implementations of the direct differentiation method. Several challenges disappear when the analysis is linear. In the analyses conducted in this section, the Rayleigh damping matrix $\mathbf{C}=c_M\mathbf{M}+c_K\mathbf{K}$ is employed with 5% damping ratio specified for the first two natural frequencies of the column. As a result, c_M=1.033 and c_K=0.001185 when the initial stiffness matrix is employed in the damping matrix. Figure 6 shows the displacement response at the top of the column, with colors identifying the degree of nonlinearity. The red color identifies increments where the first natural frequency is larger than 4.0 times the initial frequency; the magenta color identifies increments with that ratio above 2.0; the blue color identifies increments with that ratio above 1.01. The black line identifies

increments with little yielding. Figure 6 shows that significant yielding is taking place when the aforementioned ground motion is applied.

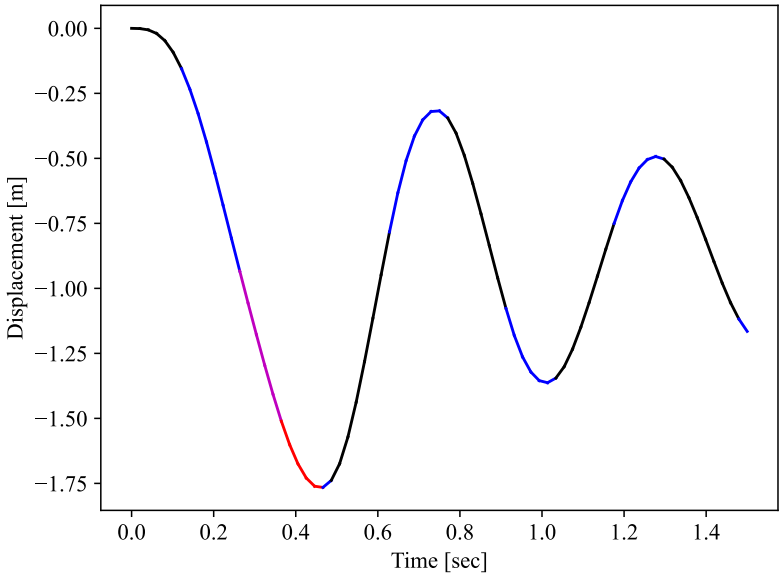

Figure 6: Displacement at the tip due to sine-wave pulse for Rayleigh damping using the initial stiffness.

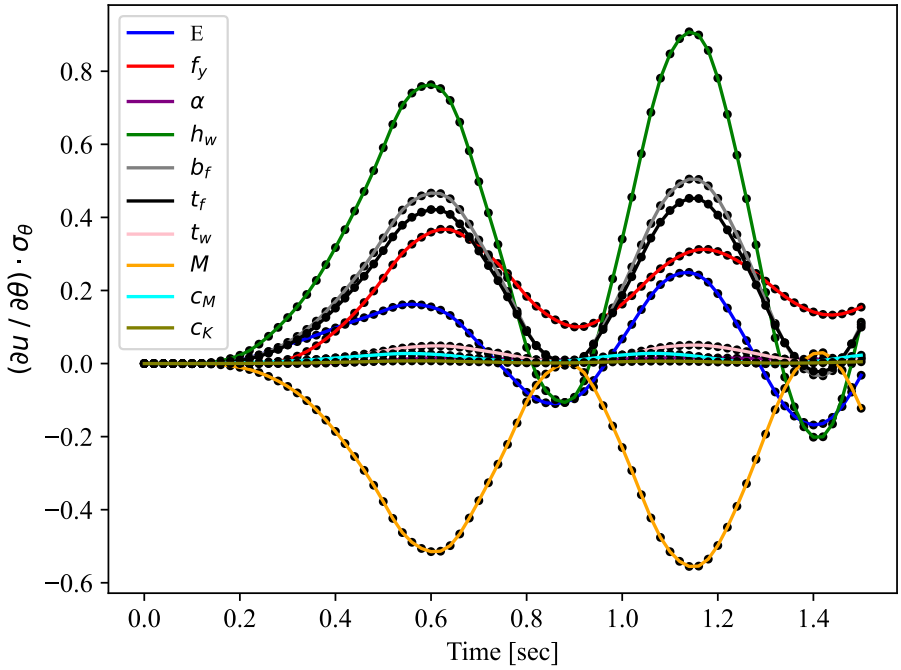

Figure 7: Response sensitivities $du/d\theta$ times σ_θ for initial-stiffness-damping and given c_M, c_K.

Figure 7 shows the displacement sensitivity results obtained for the seven parameters included in Figure 5, plus M, c_M, and c_K. As was done for the results in Figure 5, each response derivative is multiplied by the standard deviation of the respective parameter, with a 10% coefficient of variation assigned to all variables. With that scaling, the mass and the cross-section height are the two most important parameters; the former serves as a load variable; the latter serves as a resistance variable. Also, notice that c_M and c_K do not show up as important input parameters, with the given coefficients of variation. Finally, notice that Figure 7 reveal high

sensitivity of the response to parameter changes. Keeping in mind the caveat that those results are essentially local derivatives, not capturing nonlinearity, a 10% change in the value of the mass or the cross-section height would lead to a change in the response by more than 0.5m.

Figure 7 is also intended as a verification of the implementations of the direct differentiation method for nonlinear dynamic problems. As before, the black dots show results obtained by rerunning the analysis with perturbed parameter values, followed by finite difference estimation of the response derivatives. Figure 7 suggests an excellent match between the finite difference approximation and the exact results. That fact is confirmed in the analyses conducted as background work for this paper; the difference between the results obtained from the implementation of the direct differentiation method and the finite difference approximations are at least six orders of magnitude smaller than the sensitivity result. In this paper, the parameter perturbation in the finite difference analyses is set equal to 10^{-8} times the original parameter value.

7 RAYLEIGH COEFFICIENT DERIVATIVES

The derivative $d\mathbf{C}/d\theta$ appears in the right-hand side of Eq. (11). With the Rayleigh damping matrix $\mathbf{C}=c_M\mathbf{M}+c_K\mathbf{K}$, utilizing the initial stiffness matrix, that derivative reads

$$\frac{\partial \mathbf{C}}{\partial \theta} = \frac{\partial c_M}{\partial \theta}\mathbf{M} + c_M\frac{\partial \mathbf{M}}{\partial \theta} + \frac{\partial c_K}{\partial \theta}\mathbf{K} + c_K\frac{\partial \mathbf{K}}{\partial \theta} \tag{16}$$

Suppose c_M and c_K are implicitly specified by the analyst as a target damping ratio, ζ_{target}, at two natural frequencies ω_1 and ω_2. In that case [15]

$$c_M = \omega_1 \cdot \omega_2 \cdot \frac{2\cdot\zeta_{\text{target}}}{\omega_1+\omega_2} \tag{17}$$

and

$$c_K = \frac{2\cdot\zeta_{\text{target}}}{\omega_1+\omega_2} \tag{18}$$

As a result, the derivatives required in Eq. (16) are

$$\frac{\partial c_M}{\partial \theta} = \frac{\partial \omega_1}{\partial \theta}\cdot\omega_2\cdot\frac{2\cdot\zeta_{\text{target}}}{\omega_1+\omega_2} + \omega_1\cdot\frac{\partial \omega_2}{\partial \theta}\cdot\frac{2\cdot\zeta_{\text{target}}}{\omega_1+\omega_2} - \omega_1\cdot\omega_2\cdot\frac{2\cdot\zeta_{\text{target}}}{(\omega_1+\omega_2)^2}\cdot\left(\frac{\partial \omega_1}{\partial \theta}+\frac{\partial \omega_2}{\partial \theta}\right) \tag{19}$$

and

$$\frac{\partial c_K}{\partial \theta} = -\frac{2\cdot\zeta_{\text{target}}}{(\omega_1+\omega_2)^2}\cdot\left(\frac{\partial \omega_1}{\partial \theta}+\frac{\partial \omega_2}{\partial \theta}\right) \tag{20}$$

The derivatives $d\omega_1/d\theta$ and $d\omega_2/d\theta$ are obtained from the derivative of the eigenvalues γ_1 and γ_2 from the eigenvalue problem $[\mathbf{K}-\gamma\mathbf{M}]\boldsymbol{\phi}=\mathbf{0}$, where $\boldsymbol{\phi}$ is an eigenvector. Because ω is the square root of γ, the result is

$$\frac{\partial \omega}{\partial \theta} = \frac{1}{2}\cdot\frac{1}{\sqrt{\gamma}}\cdot\frac{\partial \gamma}{\partial \theta} \tag{21}$$

Before embarking on the calculation of $d\gamma/d\theta$, it is noted that the eigenvectors are scaled to unit length. As a result, the norm $||\boldsymbol{\phi}||$ equals unity and the derivative $\mathrm{d}||\boldsymbol{\phi}||/d\theta$ is zero. It can be shown that $\mathrm{d}||\boldsymbol{\phi}||/d\theta$ equals the dot product $\boldsymbol{\phi}^{\mathrm{T}}(\mathrm{d}\boldsymbol{\phi}/d\theta)$, and the fact that $\boldsymbol{\phi}^{\mathrm{T}}(\mathrm{d}\boldsymbol{\phi}/d\theta)=0$ is employed in the following. The derivative of the eigenvalues are derived by differentiating $[\mathbf{K}-\gamma\mathbf{M}]\boldsymbol{\phi}=\mathbf{0}$ with respect to θ, which yields [16]

$$\frac{d\mathbf{K}}{d\theta}\boldsymbol{\phi} - \frac{d\gamma}{d\theta}\mathbf{M}\,\boldsymbol{\phi} - \gamma\frac{d\mathbf{M}}{d\theta}\boldsymbol{\phi} + [\mathbf{K}-\gamma\,\mathbf{M}]\,\frac{d\boldsymbol{\phi}}{d\theta} = \mathbf{0} \tag{22}$$

Multiplying through by $\boldsymbol{\phi}^{\mathrm{T}}$ from the left, observing that $\boldsymbol{\phi}^{\mathrm{T}}(\mathrm{d}\boldsymbol{\phi}/d\theta)=0$, and solving for $d\gamma/d\theta$ yields

$$\frac{d\gamma}{d\theta} = \frac{\boldsymbol{\phi}^{\mathrm{T}}\frac{d\mathbf{K}}{d\theta}\boldsymbol{\phi} - \gamma\boldsymbol{\phi}^{\mathrm{T}}\frac{d\mathbf{M}}{d\theta}\boldsymbol{\phi}}{\boldsymbol{\phi}^{\mathrm{T}}\mathbf{M}\,\boldsymbol{\phi}} \tag{23}$$

Figure 8 is offered to verify that result, with black dots representing finite difference results, and to gain insight into the importance of the target damping. Again, an excellent match between direct differentiation and finite difference results are observed in the figure and in the background analyses for this paper. As observed earlier for c_M and c_K, the target damping does not appear as an important variable for the 10% coefficient of variation that is assigned uniformly to all parameters.

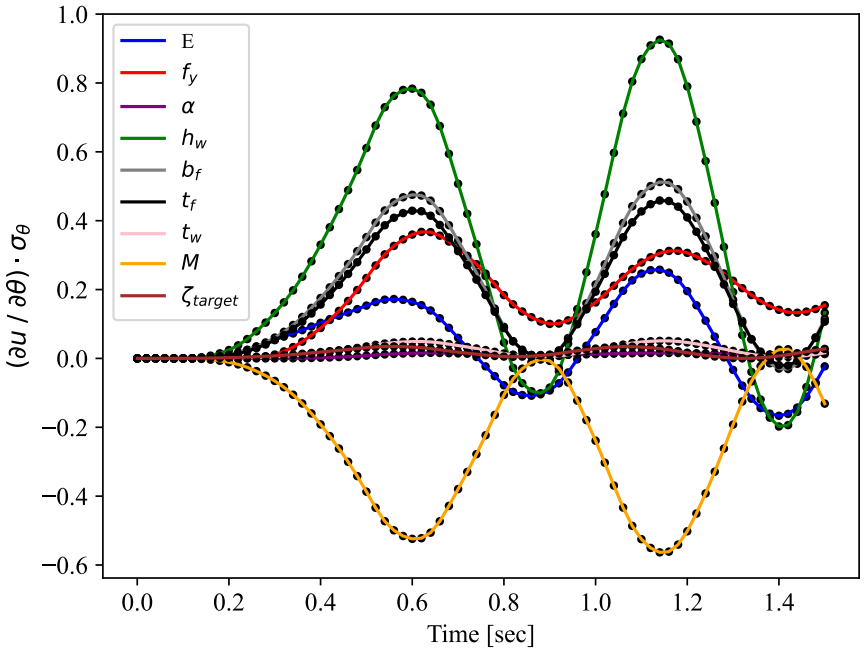

Figure 8: $du/d\theta \cdot \sigma_\theta$ for initial-stiffness-damping and use of eigenvalues to calculate c_M and c_K.

8 RAYLEIGH MATRIX DERIVATIVES, PART I

Now consider the case where the Rayleigh damping matrix is formulated in terms of the current tangent stiffness matrix:

$$\mathbf{C} = c_M\mathbf{M} + c_K\mathbf{K}(\mathbf{u}(\theta),\theta) \tag{24}$$

where the implicit dependence on θ via $\mathbf{u}$ is highlighted, together with the potential explicit dependence on θ via the algorithm that forms $\mathbf{K}$. Before proceeding, the displacement response with that damping scheme is displayed in Figure 9. As expected, the maximum displacement is now somewhat larger than what is displayed in Figure 6. That is the result of the lower damping associated with the lower current tangent stiffness. Differentiation of the damping matrix in Eq. (24) yields

$$\frac{\partial\mathbf{C}}{\partial\theta} = \frac{\partial c_M}{\partial\theta}\mathbf{M} + c_M\frac{\partial\mathbf{M}}{\partial\theta} + \frac{\partial c_K}{\partial\theta}\mathbf{K} + c_K\left(\frac{\partial\mathbf{K}}{\partial\mathbf{u}_{n+1}}\frac{\partial\mathbf{u}_{n+1}}{\partial\theta} + \left.\frac{\partial\mathbf{K}(\mathbf{u}_{n+1})}{\partial\theta}\right|_{\mathbf{u}\text{ fixed}}\right) \tag{25}$$

The appearance of the third-order tensor $d\mathbf{K}/d\mathbf{u}$ is unusual in structural analysis. It appears because of the implicit dependence on θ via $\mathbf{u}$. In fact, Eq. (25) shows that the elements, sections, and materials must produce $d\mathbf{K}/d\mathbf{u}$, in addition to the conditional derivative $d\mathbf{K}/d\theta$. That

challenge is addressed in the next section for the Bouc-Wen model; the presence of $d\mathbf{K}/d\mathbf{u}$ is the primary reason why that material model is selected for this paper. For a bilinear model, the result would be $d\mathbf{K}/d\mathbf{u}=\mathbf{0}$ because the displacement would not affect the stiffness in the infinitesimal vicinity of any strain value, whether the response is elastic or plastic. Conversely, a material model with a nonlinear stress-strain curve, such as the Bouc-Wen model, will have $d\mathbf{K}/d\mathbf{u}\neq\mathbf{0}$.

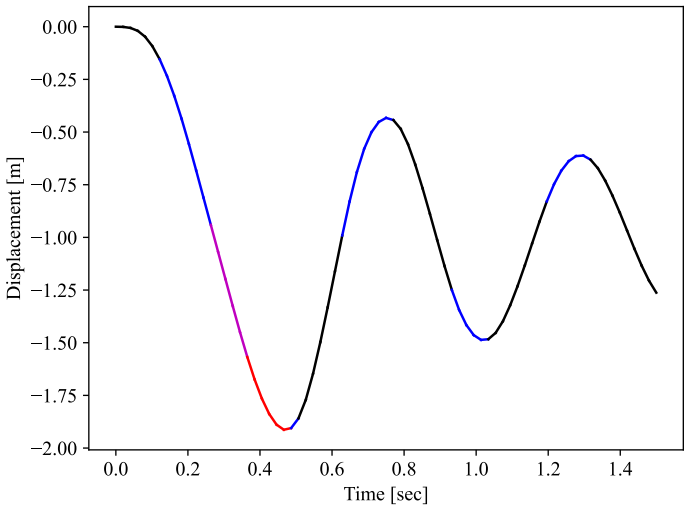

Figure 9: Displacement response for Rayleigh damping with current tangent stiffness.

Eq. (25) raises another issue; the sought response sensitivity $d\mathbf{u}/d\theta$ appears in $d\mathbf{C}/d\theta$, and therefore in the right-hand side of Eq. (11). Recall that Eq. (11) is a system of equations intended to be solved for exactly $d\mathbf{u}/d\theta$. This means that the portion of Eq. (25) with $d\mathbf{u}/d\theta$ must be moved to the left-hand side of Eq. (11). To accomplish that, two steps are taken. First, the part of Eq. (25) that contains $d\mathbf{u}/d\theta$ is substituted into the relevant term in the right-hand side of Eq. (11). That term is a vector here denoted by the symbol $\mathbf{b}$:

$$\mathbf{b} = -c_K \frac{\partial \mathbf{K}}{\partial \mathbf{u}_{n+1}} \frac{\partial \mathbf{u}_{n+1}}{\partial \theta} (a_5 \mathbf{u}_{n+1} + a_6 \mathbf{u}_n + a_7 \dot{\mathbf{u}}_n + a_8 \ddot{\mathbf{u}}_n) \tag{26}$$

Index notation is helpful when isolating $d\mathbf{u}/d\theta$ in order to have the remainder serve as the modification to the coefficient matrix in Eq. (11):

$$b_i = -c_K \left(\frac{\partial \mathbf{K}}{\partial \mathbf{u}_{n+1}}\right)_{imj} \left(\frac{\partial \mathbf{u}_{n+1}}{\partial \theta}\right)_j (a_5 \mathbf{u}_{n+1} + a_6 \mathbf{u}_n + a_7 \dot{\mathbf{u}}_n + a_8 \ddot{\mathbf{u}}_n)_m =$$

$$= -\left[c_K \left(\frac{\partial \mathbf{K}}{\partial \mathbf{u}_{n+1}}\right)_{imj} (a_5 \mathbf{u}_{n+1} + a_6 \mathbf{u}_n + a_7 \dot{\mathbf{u}}_n + a_8 \ddot{\mathbf{u}}_n)_m\right] \left(\frac{\partial \mathbf{u}_{n+1}}{\partial \theta}\right)_j \tag{27}$$

The square bracket contains the amendment to the effective stiffness, i.e., the coefficient matrix in Eq. (11). Importantly, Eq. (27) shows that the parenthesis $(a_5 \mathbf{u}_{n+1} + a_6 \mathbf{u}_n + a_7 \dot{\mathbf{u}}_n + a_8 \ddot{\mathbf{u}}_n)$ is contracted with the middle index of the third-order tensor $\partial\mathbf{K}/\partial\mathbf{u}$. That amendment is implemented in G2, together with the derivations in the next section, in order to obtain correct response sensitivities in nonlinear dynamics with Rayleigh damping specified in terms of the current tangent stiffness. In passing, it is noted that this development also amends a somewhat imprecise statement made by the author near Eq. (24) in [17]. Rayleigh damping with current tangent stiffness does not lead to a nonlinear system of equations for the response sensitivities; rather, the coefficient matrix must be adjusted as described above.

9 BOUC-WEN DERIVATIVES, PART II

The previous section reveals the need for $d\mathbf{K}/d\mathbf{u}$ and $d\mathbf{K}/d\theta$, the latter conditional on fixed current displacements. At the material level, this prompts the calculation of the derivative of the stiffness, $d\sigma_{n+1}/d\varepsilon_{n+1}$, and therefore $dz_{n+1}/d\varepsilon_{n+1}$, with respect to ε_{n+1} and also with respect to θ, the latter for fixed ε_{n+1}. Earlier in this paper, Eq. (5) was differentiated with respect to ε_{n+1} in order to obtain the algorithmically consistent tangent stiffness. That derivative is now differentiated again, separately with respect to ε_{n+1} and θ. The resulting expressions for $d(dz_{n+1}/d\varepsilon_{n+1})/d\varepsilon_{n+1}$ and $d(dz_{n+1}/d\varepsilon_{n+1})/d\theta$ are implemented in G2 in order to obtain the results presented shortly.

10 SECTION DERIVATIVES, PART II

The point made earlier in regards to the differentiation of the section integration in Eq. (14) is here reiterated for the calculation of $d\mathbf{K}/d\theta$. The importance of this point relates to situations where θ is a cross-section parameter that affects the transformation $\varepsilon=\mathbf{T}_{ms}\mathbf{u}_s$. The section integration to calculate the section stiffness reads

$$\mathbf{K}_s = \sum_{j=1}^{N_{\text{fib}}} (\mathbf{T}_{ms}^{\text{T}} \mathbf{T}_{ms} \cdot A \cdot \sigma) \tag{28}$$

The derivative sought in the last term in Eq. (25) is, when θ is a section parameter:

$$\left.\frac{\partial \mathbf{K}_s}{\partial \theta}\right|_{\mathbf{u}_{s,n+1}\text{ fixed}} = \sum_{j=1}^{N_{\text{fib}}} \left(\begin{array}{c} \frac{\partial \mathbf{T}_{ms}}{\partial \theta} \mathbf{T}_{ms} \cdot A \cdot \frac{\partial \sigma_{n+1}}{\partial \varepsilon_{n+1}} + \mathbf{T}_{ms} \frac{\partial \mathbf{T}_{ms}}{\partial \theta} \cdot A \cdot \frac{\partial \sigma_{n+1}}{\partial \varepsilon_{n+1}} \\ + \mathbf{T}_{ms} \cdot \frac{\partial A}{\partial \theta} \cdot \frac{\partial \sigma_{n+1}}{\partial \varepsilon_{n+1}} + \mathbf{T}_{ms}^{\text{T}} \mathbf{T}_{ms} \cdot A \cdot \left(\frac{\partial \left(\frac{\partial \sigma_{n+1}}{\partial \varepsilon_{n+1}}\right)}{\partial \varepsilon_{n+1}} \cdot \frac{\partial \varepsilon_{n+1}}{\partial \theta} + \left.\frac{\partial \left(\frac{\partial \sigma_{n+1}}{\partial \varepsilon_{n+1}}\right)}{\partial \theta}\right|_{\varepsilon_{n+1}\text{ fixed}} \right) \end{array} \right) \tag{29}$$

where the derivative of the stiffness with respect to the strain, an unusual quantity in structural analysis, appears. Figure 10, the result of nonlinear dynamic analysis, shows displacement derivatives with respect to h_w. The figure highlights the importance of including the somewhat unusual derivatives $d(d\sigma_{n+1}/d\varepsilon_{n+1})/d\varepsilon_{n+1}$ and $d(d\sigma_{n+1}/d\varepsilon_{n+1})/d\theta$ in order to calculate correct response sensitivities. With those quantities included, the blue line in Figure 10 matches perfectly the finite difference result, shown as black dots. Conversely, missing the aforementioned derivatives in Eq. (29) yields the erroneous red line in Figure 10.

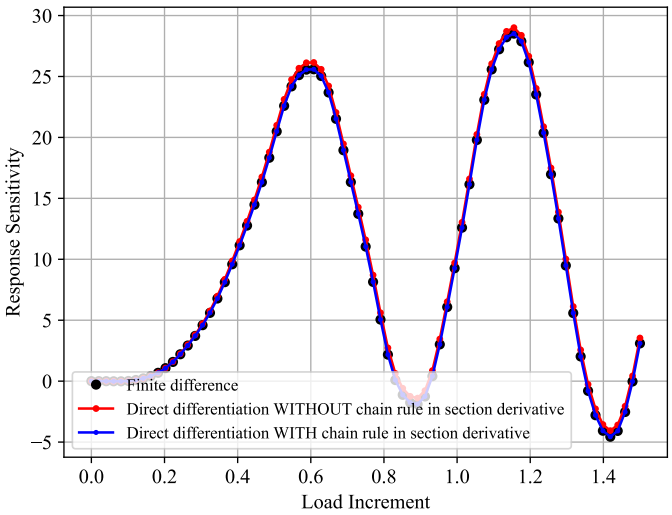

Figure 10: Inaccuracy in response sensitivity result when missing the chain rule of differentiation in Eq. (29).

11 RAYLEIGH MATRIX DERIVATIVES, PART II

The use of the current tangent stiffness in Rayleigh damping has an additional consequence when c_M and c_K are implicitly specified as a target damping ratio, ζ, at two natural frequencies ω_1 and ω_2. The earlier derivations are now extended to include the implicit dependence of θ via the displacement vector. Differentiation of c_M yields

$$\frac{\partial c_M}{\partial \theta} = \left(\frac{\partial c_M}{\partial \omega_1}\cdot\frac{\partial \omega_1}{\partial \gamma_1}\cdot\frac{\partial \gamma_1}{\partial \mathbf{K}} + \frac{\partial c_M}{\partial \omega_2}\cdot\frac{\partial \omega_2}{\partial \gamma_2}\cdot\frac{\partial \gamma_2}{\partial \mathbf{K}}\right)\cdot\frac{\partial \mathbf{K}}{\partial \mathbf{u}}\cdot\frac{\partial \mathbf{u}}{\partial \theta} + \left.\frac{\partial c_M}{\partial \theta}\right|_{\mathbf{u}\text{ fixed}} \tag{30}$$

and differentiation of c_K yields

$$\frac{\partial c_K}{\partial \theta} = \left(\frac{\partial c_K}{\partial \omega_1}\cdot\frac{\partial \omega_1}{\partial \gamma_1}\cdot\frac{\partial \gamma_1}{\partial \mathbf{K}} + \frac{\partial c_K}{\partial \omega_2}\cdot\frac{\partial \omega_2}{\partial \gamma_2}\cdot\frac{\partial \gamma_2}{\partial \mathbf{K}}\right)\cdot\frac{\partial \mathbf{K}}{\partial \mathbf{u}}\cdot\frac{\partial \mathbf{u}}{\partial \theta} + \left.\frac{\partial c_K}{\partial \theta}\right|_{\mathbf{u}\text{ fixed}} \tag{31}$$

All derivatives required in Eqs. (30) and (31) are presented earlier, except the derivative of the eigenvalues with respect to the current stiffness matrix, i.e., $d\gamma/d\mathbf{K}$. In fact, the conditional derivatives in the last term of Eqs. (30) and (31) are presented earlier in Eqs. (19) and (20). In order to obtain $d\gamma/d\mathbf{K}$, it is again helpful to employ index notation. The eigenvalue problem then reads

$$\left[K_{ij} - \gamma M_{ij}\right]\phi_j = 0 \tag{32}$$

Differentiating through with respect to the stiffness matrix yields

$$\frac{d}{dK_{kl}}\left(\left[K_{ij} - \gamma M_{ij}\right]\phi_j\right) = \left[\frac{dK_{ij}}{dK_{kl}} - \frac{d\gamma}{dK_{kl}}M_{ij} - \gamma\frac{dM_{ij}}{dK_{kl}}\right]\phi_j + \left[K_{ij} - \gamma M_{ij}\right]\frac{d\phi_j}{dK_{kl}} = 0 \tag{33}$$

Multiplying from the left by the transpose of the eigenvector causes the last term to vanish, as before, with the result

$$\phi_i\frac{dK_{ij}}{dK_{kl}}\phi_j - \phi_i\frac{d\gamma}{dK_{kl}}M_{ij}\,\phi_j - \phi_i\gamma\frac{dM_{ij}}{dK_{kl}}\phi_j = 0 \tag{34}$$

where the "identity matrix" is recognized in the first term:

$$\phi_i I_{ij,kl}\phi_j - \phi_i\frac{d\gamma}{dK_{kl}}M_{ij}\,\phi_j - \phi_i\gamma\frac{dM_{ij}}{dK_{kl}}\phi_j = 0 \tag{35}$$

The derivative of the mass with respect to stiffness, in the last term, is zero in practical situations. The product $\phi_i I_{ij,kl}\phi_j$ results in a matrix formed by the outer product of the eigenvector with itself. Solving for the sought derivative yields

$$\frac{d\gamma}{dK_{kl}} = \frac{\phi_k\phi_l}{\phi_i M_{ij}\,\phi_j} \tag{36}$$

In vector-matrix notation, that result reads

$$\frac{d\gamma}{d\mathbf{K}} = \frac{\boldsymbol{\phi}\boldsymbol{\phi}^{\mathrm{T}}}{\boldsymbol{\phi}^{\mathrm{T}}\mathbf{M}\,\boldsymbol{\phi}} \tag{37}$$

Eqs. (30) and (31) represent yet another case where the sought response sensitivity, $d\mathbf{u}/d\theta$, appears in the right-hand side of Eq. (11). Index notation is again employed, albeit not shown here for brevity, to demonstrate the following: 1) The amendment to the coefficient matrix of the response sensitivity system is the outer product of two vectors; 2) The first vector is obtained by a contraction of the first two indices of $d\mathbf{K}/d\mathbf{u}$ with the two indices of $d\gamma/d\mathbf{K}$; 3) The second vector is obtained from the matrix-vector product of the mass matrix with the parenthesis that contains a_5, presented earlier. Interestingly, the resulting correction of the coefficient matrix in the system of equations for $d\mathbf{u}/d\theta$ is asymmetric. This fact is verified in the background analyses

for this paper, with a perfect match obtained with finite difference results once the previous equations are correctly implemented. Figures are not included here because they look very similar to Figure 7 and Figure 8.

12 MODAL DAMPING

Several problems are associated with the use of Rayleigh damping in nonlinear dynamic analysis. That is the case regardless of whether the initial stiffness or the current tangent stiffness is included [18][19][20]. Chopra and McKenna [20] identify the benefits of employing the modal damping matrix instead, which reads

$$\mathbf{C} = \mathbf{M}\left(\sum_{j=1}^{N} \frac{2\zeta_j \omega_j}{m_j} \boldsymbol{\phi}_j \boldsymbol{\phi}_j^{\mathrm{T}}\right)\mathbf{M} \tag{38}$$

where N is here the number of modes, ζ_j is the imposed damping ratio at mode j, ω_j is the natural frequency of vibration in mode j, $\boldsymbol{\phi}_j$ is the corresponding mode shape, and m_j is the modal mass, i.e., $\boldsymbol{\phi}_j^{\mathrm{T}}\mathbf{M}\boldsymbol{\phi}_j$. The objective now is to calculate the derivative $\partial\mathbf{C}/\partial\theta$, where θ is an input parameter to the finite element model. The product rule of differentiation yields

$$\begin{aligned}\frac{d\mathbf{C}}{d\theta} &= \frac{d\mathbf{M}}{d\theta}\left(\sum_{j=1}^{N} \frac{2\zeta_j \omega_j}{m_j} \boldsymbol{\phi}_j \boldsymbol{\phi}_j^{\mathrm{T}}\right)\mathbf{M} \\ &+\mathbf{M}\left(\sum_{j=1}^{N} \frac{2\zeta_j \frac{d\omega_j}{d\theta}}{m_j} \boldsymbol{\phi}_j \boldsymbol{\phi}_j^{\mathrm{T}}\right)\mathbf{M} - \mathbf{M}\left(\sum_{j=1}^{N} \frac{2\zeta_j \omega_j}{m_j^2} \cdot \frac{dm_j}{d\theta} \cdot \boldsymbol{\phi}_j \boldsymbol{\phi}_j^{\mathrm{T}}\right)\mathbf{M} \\ &+\mathbf{M}\left(\sum_{j=1}^{N} \frac{2\zeta_j \omega_j}{m_j} \cdot \frac{d\boldsymbol{\phi}_j}{d\theta} \boldsymbol{\phi}_j^{\mathrm{T}}\right)\mathbf{M} + \mathbf{M}\left(\sum_{j=1}^{N} \frac{2\zeta_j \omega_j}{m_j} \boldsymbol{\phi}_j \frac{d\boldsymbol{\phi}_j^{\mathrm{T}}}{d\theta}\right)\mathbf{M} \\ &+\mathbf{M}\left(\sum_{j=1}^{N} \frac{2\zeta_j \omega_j}{m_j} \boldsymbol{\phi}_j \boldsymbol{\phi}_j^{\mathrm{T}}\right)\frac{d\mathbf{M}}{d\theta}\end{aligned} \tag{39}$$

where $dm_j/d\theta = (d\boldsymbol{\phi}_j/d\theta)^{\mathrm{T}}\mathbf{M}\boldsymbol{\phi}_j + \boldsymbol{\phi}_j^{\mathrm{T}}(d\mathbf{M}/d\theta)\boldsymbol{\phi}_j + \boldsymbol{\phi}_j^{\mathrm{T}}\mathbf{M}(d\boldsymbol{\phi}_j/d\theta)$. The derivative of the mass matrix is usually trivial and the derivative of eigenvalues and eigenvectors are developed in previous sections. Plots are not presented in this section for brevity, but Eq. (39) is implemented in G2 and the results are verified by means of finite difference calculations. The reason why plots are omitted is that, when the initial stiffness matrix is employed in the eigenvalue problem to determine γ and $\boldsymbol{\phi}$, the displacement response is essentially the same as in Figure 6, presented earlier. Furthermore, the sensitivity results are essentially the same as in Figure 8.

13 APPLICATIONS

Gradient-based algorithms, employed in design optimization and the first-order reliability method, are direct applications of the response sensitivities derived in this paper. However, one may argue that all nonlinear dynamic analyses should be accompanied by considerations of response sensitivities. A few examples are suggested in the following sections.

13.1 Importance Ranking of Input Parameters

One obvious application of response sensitivity results is displayed in Figure 5, Figure 7, and Figure 8. Those plots show the evolution in the response sensitivities with time, or pseudo-time for static analysis. However, in those plots, the choice of 10% coefficient of variation for all parameters is not realistic. Denoting a coefficient of variation by the symbol δ, the somewhat

more realistic choices δ_E=10%, δ_{fy}=20%, δ_α=20%, δ_{hw}=2%, δ_{bf}=2%, δ_{tf}=2%, δ_{tw}=2%, δ_M=20%, and $\delta_{targetDamping}$=20% give a new version of Figure 8, shown in Figure 11. The analysis is continued until 3 seconds, for the same sine pulse as described earlier, for the sake of this illustration. As explained on Page 39 of the book by Der Kiureghian [21], $(du/d\theta)\sigma_\theta$, displayed in Figure 11 and earlier, is a basic importance measure for the ranking input parameters. Figure 11 reveals that the mass and the yield stress are the most important input parameters, with opposite effect on the displacement. Also note that even parameters such as the modulus of elasticity and the cross-section height rank above the target damping in importance.

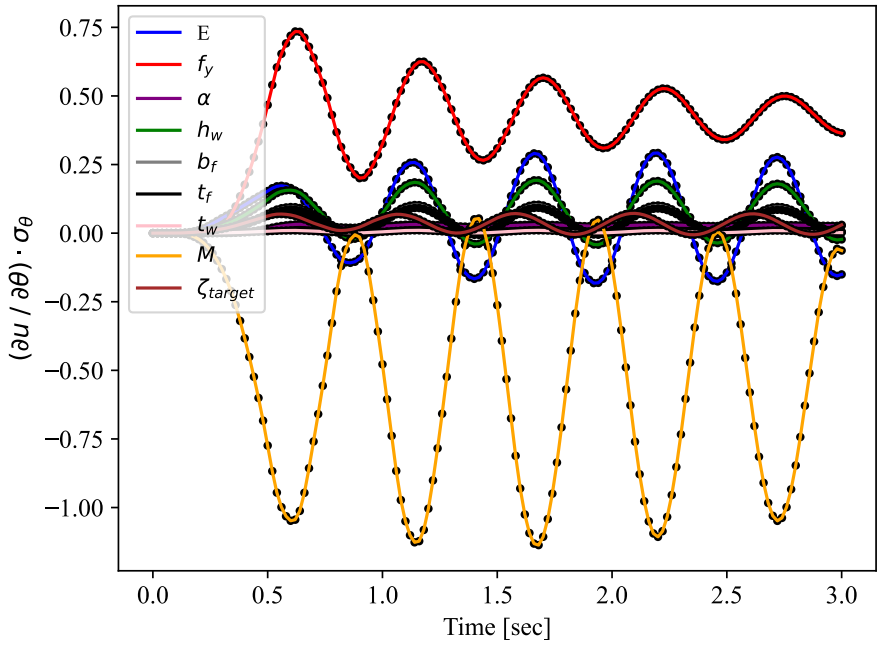

Figure 11: New version of Figure 8 with updated σ_θ-values.

13.2 Response Standard Deviation

Another application of response sensitivities calculated alongside the response is the estimation of the standard deviation of the response. In the absence of correlation, an approximation of the standard deviation based on a Taylor linearization of the displacement is the square root of the sum of squared values in Figure 11. See for example Section 2.9 in [21]. The result is shown in Figure 12. The result in Figure 12 is produced with Rayleigh damping with the initial stiffness, and the uniform 10% coefficients of variation for all parameters. In Figure 6, presented earlier, the average displacement is roughly 0.8m with a maximum displacement of 1.75m. Considering uncertainty in all of E, f_y, α, h_w, b_f, t_f, t_w, M, and ζ_{target} the resulting standard deviation of the response is displayed in Figure 12. The average standard deviation of the response, as well as the maximum standard deviation, are near the average and maximum displacement. That high value of the standard deviation stems from the high sensitivity remarked below Figure 7.

13.3 Actual Ground Motion

A comment related to the coefficient of variation of the response is added by subjecting the column in Figure 1 to the well-known El Centro ground motion, here scaled to a peak ground acceleration of 3g in order to observe nonlinear structural behaviour. Repeating the analysis setup with 10% coefficient of variation for all nine uncorrelated input parameters, plus Rayleigh damping with the initial stiffness matrix, produces the displacement response shown in Figure

13. If that response is considered as a stochastic process, then its standard deviation is varying at levels below approximately 0.2m. However, that standard deviation is not what is discussed in the previous section. Rather, the coefficient of variation gleaned from Figure 13 is a result of the energy, i.e., variance of the ground motion. Conversely, the coefficient of variation discussed in the previous section and plotted in Figure 14 for the El Centro ground motion is the standard deviation of the function $u(\mathbf{x})$, where $\mathbf{x}$ is the vector containing the nine input random variables. Figure 14 matches the observation made in the previous section, showing response standard deviations of the same order of magnitude as the response.

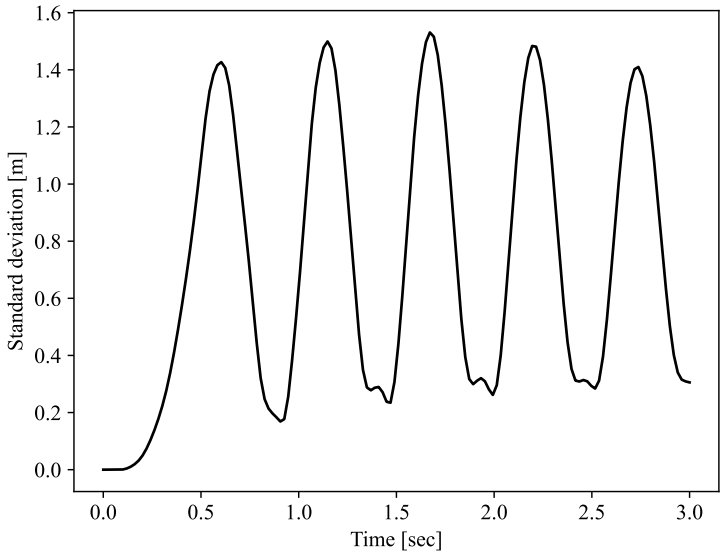

Figure 12: Standard deviation of the displacement, as a function of time, using the values in Figure 11.

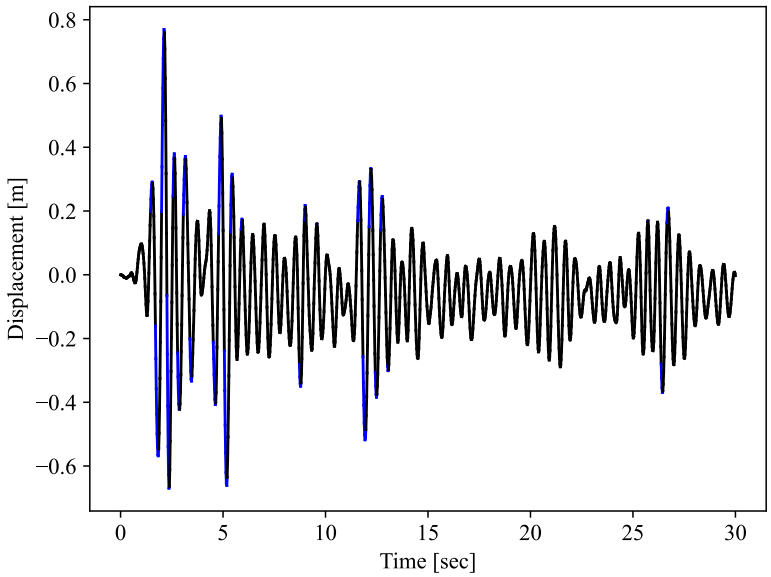

Figure 13: Displacement at the tip of the column subjected to the scaled El Centro ground motion.

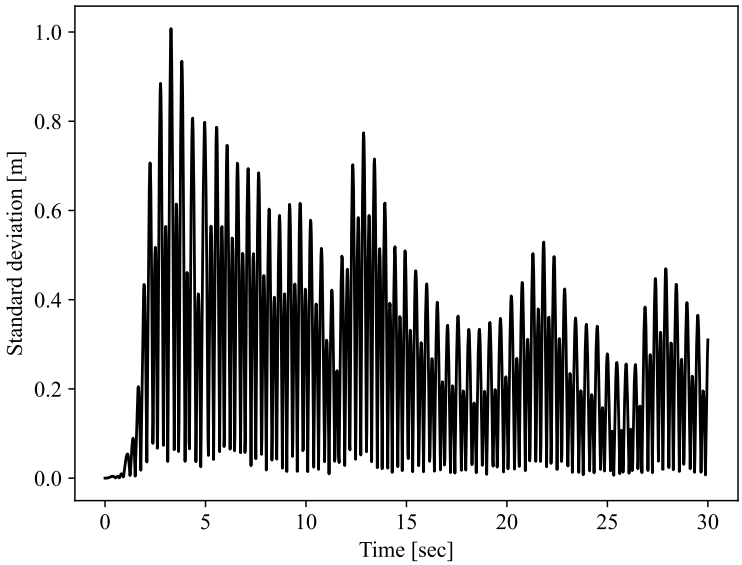

Figure 14: Standard deviation of the displacement for the scaled El Centro ground motion.

14 CONCLUSIONS

A viscous damping matrix is needed in nonlinear dynamic analysis of structures. Several options exist. A common choice is Rayleigh damping, in which the damping matrix is a weighted sum of the mass matrix and either the initial stiffness matrix or the current stiffness matrix. The modal damping matrix serves as yet another alternative. This paper presents derivations, implementations, and calculations of exact response sensitivities when any of the those damping models are employed. The direct differentiation method is adopted; that means the governing response equations are analytically differentiated and implemented alongside the response algorithm. The three-dimensional tensor formed by differentiation of the stiffness matrix with respect to the displacement vector appear in the derivations. So does the derivative of the eigenvalues with respect to the input parameters. Results are presented in this paper to verify the response sensitivity implementations and to suggest applications for such results.

REFERENCES

[1] Choi, K. K., Santos, J. L. T., Yao, T.-M. (1988). “Recent advances in design sensitivity analysis and its use in structural design process.” SAE Transactions, 97(5), 181-197.

[2] Arora, J. S. & Cardoso, J. B. (1989). “A design sensitivity analysis principle and its implementation into ADINA.” Computers & Structures, 43(3/4), 691-705.

[3] Tsay, J. J. & Arora, J. S. (1990). “Nonlinear structural design sensitivity analysis for path dependent problems. Part 1: General Theory.” Computer Methods in Applied Mechanics and Engineering, 81, 183-208.

[4] Tsay, J. J. & Arora, J. S. (1990). “Nonlinear structural design sensitivity analysis for path dependent problems. Part 2: Analytical Examples.” Computer Methods in Applied Mechanics and Engineering, 81, 209-228.

[5] Cardoso, J. B. & Arora, J. S. (1992). "Design sensitivity analysis of nonlinear dynamic response of structural and mechanical systems." Structural Optimization, 4, 37-46.

[6] Zhang, Y. & Der Kiureghian, A. (1993). "Dynamic response sensitivity of inelastic structures." Computer Methods in Applied Mechanics and Engineering, 108, 23-36.

[7] Haukaas, T. & Der Kiureghian, A. (2003). "Finite element reliability and sensitivity methods for performance-based earthquake engineering" Pacific Earthquake Engineering Research (PEER) Center Report No. 2003/14.

[8] Scott, M. H., Franchin, P., Fenves, G. L., Filippou, F. C. (2004). "Response sensitivity for nonlinear beam-column elements." ASCE Journal of Structural Engineering, 130(9), 1281-1288.

[9] Baber, T. T. & Noori, M. N. (1985). "Random vibration of degrading, pinching systems." ASCE Journal of Engineering Mechanics, 111(8), 1010–1026.

[10] McKenna, F., Scott, M. H., Fenves, G. L. (2010). "Nonlinear finite-element analysis software architecture using object composition." ASCE Journal of Computing in Civil Engineering, 24(1), 95-107.

[11] Schellenberg, A. H, Sarebanha, A., Schoettler, M. J., Mosqueda, G., Benzoni, G., Mahin, S. A. (2015). "Hybrid simulation of seismic isolation systems applied to an APR-1400 nuclear power plant." Pacific Earthquake Engineering Research (PEER) Center Report No. 2015/05.

[12] Casciati, F. (1989). "Stochastic dynamics of hysteretic media." Structural Safety, 6, 259-269.

[13] Wen, Y.-K. (1976). "Method for random vibration of hysteretic systems." ASCE Journal of Engineering Mechanics, 102(2), 249–263.

[14] Baber, T. T. & Wen, Y.-K. (1981). "Random vibration of hysteretic degrading systems." ASCE Journal of Engineering Mechanics, 107(6), 1069-1087.

[15] Chopra, A. K. (1995). Dynamics of structures: Theory and applications to earthquake engineering." Prentice Hall.

[16] Magnus, J. (1985). "On differentiating eigenvalues and eigenvectors." Econometric Theory, 1, 1790191.

[17] Haukaas, T. & Der Kiureghian, A. (2005). "Parameter sensitivity and importance measures in nonlinear finite element reliability analysis." ASCE Journal of Engineering Mechanis, 131(10), 1013-1026.

[18] Hall, J. F. (2006). "Problems encountered from the use (or misuse) of Rayleigh damping." Earthquake Engineering & Structural Dynamics, 35, 525-545.

[19] Carney, F. A. (2008). "Unintended consequences of modeling damping in structures." ASCE Journal of Structural Engineering, 134(4), 581-592.

[20] Chopra, A. K. & McKenna, F. (2016). "Modeling viscous damping in nonlinear response history analysis of buildings for earthquake excitation." Earthquake Engineering & Structural Dynamics, 45, 193-211.

[21] Der Kiureghian, A. (2022). "Structural and System Reliability." Cambridge University Press.